- Technical Paper -

STRUCTURAL DAMAGES OF BEAMS IN MULTI-STORY RC SHEAR WALLS WITH MULTIPLE DOOR OPENINGS

Rado RAMAROZATOVO[*1]・Minori HIROSAWA[*1]・Takuya KINOSHITA[*2]・Toshikatsu ICHINOSE[*3]

ABSTRACT

This paper reports the test results of two 1/4 scale 3-story shear wall specimens subjected to cyclic loadings. One of the specimen had diagonally aligned openings and the other had vertically aligned openings. The displacements of the beams around the openings were measured using digital cameras. The deformations obtained at the intermediate floors of the specimen with vertically aligned openings, which showed the most brittle behavior, were concentrated in the areas between the openings. Those of the specimen with diagonally aligned openings, with more ductile behavior, were widely distributed.

Keywords: multi-story RC shear wall, door openings, reduction factor, shear crack

1. INTRODUCTION

The RC building code of AIJ [1] includes a shear strength reduction factor to assess the effect of door openings in a wall. The shear strength of a wall is expected to be evaluated multiplying the factor and the strength of a wall without such openings. To study the validity of the factor, an experiment was conducted on three 3-story specimens and reported in Ref. [2]. Two of the specimens had openings as shown in Fig.1. The remaining specimen had no opening. This paper discusses the deformation of the beams shown in Fig.1, which was measured using digital cameras. The application of digital cameras for as a measurement tool is called noncontact measurement method, and is generally adopted in Digital Image Correlation (DIC) [3] or during structural researches to monitor displacements, when contact measurement methods (differential transducer, strain gauge,...) cannot be used. The application process of such measurement method will be developed in the following sections, as well as the results of the monitoring of the beams at the 3rd and the roof floors.

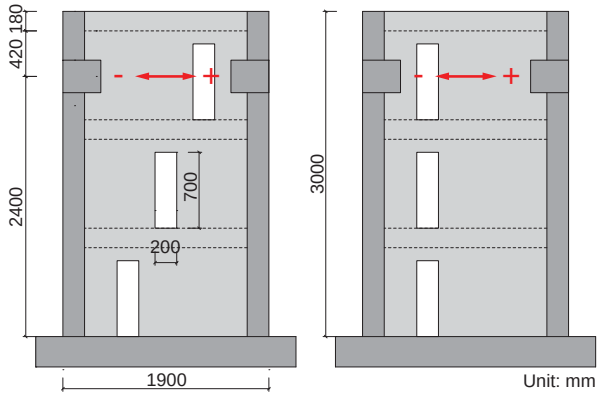

a) WD1 b) WV1

Fig. 1 Dimensions of the specimens

2. SPECIMEN DESIGN

The two 3-story specimens selected for the study had a height-to-length ratio of 1.6, a scale of 1/4, and dimensions of: Length(l_w)=1700mm, height(h_w)=3000mm, thickness(t_w)=60mm. They were built with boundary columns of 200x180mm section. As displayed in Fig.1, the two specimens, named WD1 and WV1, were designed with aligned door openings of 200mm wide and 700mm high at each floor. The alignments of the openings were respectively, diagonal and vertical. Two separated beams were added at 2400m height to apply the reverse static shear load. The directions of the loadings, positive and negative are shown by the red double arrows in Fig.1.

*1 Graduate Student, Dept. of Social Engineering, Nagoya Institute of Technology
*2 Undergraduate Student, Dept. of Architecture and Design, Nagoya Institute of Technology
*3 Prof., Graduate School of Engineering, Nagoya Institute of Technology, Dr. Eng.

The results of the shear capacities of the test specimens are gathered in the Shear-load-versus-drift envelope curves in Fig.2. WD1 shows the biggest performances, though the test results differ by approximately 10% from the computation of maximum shear capacity considering the reduction factor.

In WV1 however, the overestimation of the shear capacity is 20% and 53% at respectively negative and positive loading.

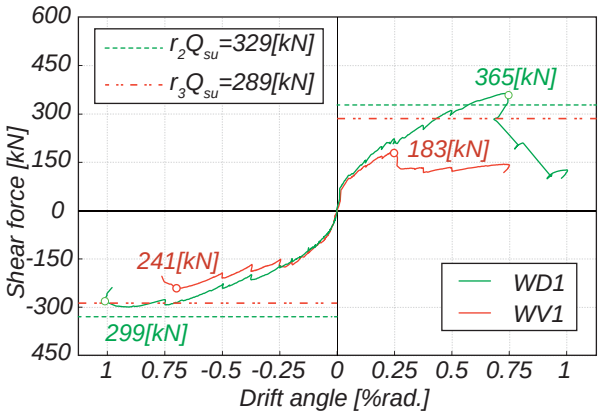

Fig. 2 Shear load-drift relationship envelope curves

3. MEASUREMENT USING DIGITAL CAMERAS

3.1 Cameras Setup

The monitoring of the deformation of the beams was set by 5152x3864 pixels digital cameras with 24 x 420mm lens. For an optimal view, two cameras were used to target the beam at each floor of the three-storied specimens. They were set side-by-side at approximately 6.00m from the specimen. The photos taken by those two cameras are referred as "left photo" and "right photo" (see Fig.3). In order to track the displacements, 10x10mm square shaped targets, designed with 2.5mm interval grids, were put on the beams (see Fig.4). The targets were placed at several places of the beam above each opening as shown in Fig.5. The same targets were put on a wooden board placed independently behind the specimen (later referred as background targets), which was supposed to be motionless. The motionless board serves as reference to measure the displacements of the targets on the specimen. The photos were taken before the loading and at the peak of each loading cycle.

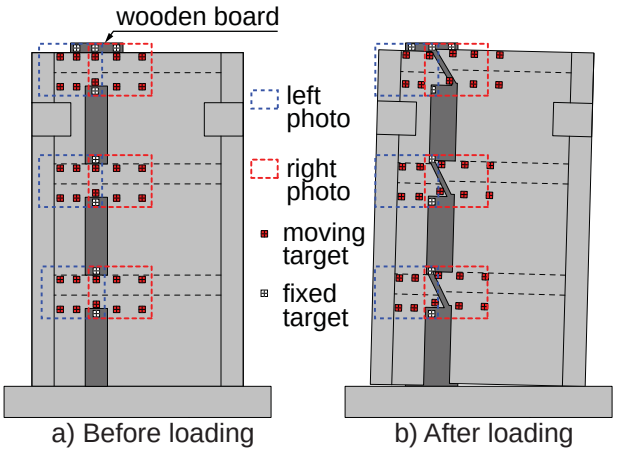

Fig. 3 Photos before loading - Top floor - WD1

3.2 Data Treatment

In order to collect the coordinates of the targets, the photos had to go through a treatment which consisted of two phases: The treatment of the photos before loading and the treatment of the photos after loading.

The treatment of the photos before loading consisted of 4 steps, illustrated in Fig.6 and described as follows: (a) Scale graphically the photos to match them with the real dimensions of the specimen. (b) Check the verticality/horizontality of the grids drawn on the specimen. (c) Correct the rotation and the scale of the left and right photos to match their positions and sizes. This step is done by matching the common targets, shown in Fig.5. (d) Define a target from the motionless background as the origin $0(X_0, Y_0)$ of coordinates and collect the coordinates of all the targets on the specimen and on the background. The coordinates of the targets before loading are labelled: ${}_B X_i$, ${}_B Y_i$.

The photos after loadings had to follow

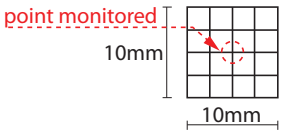

Fig. 4 Detail of a target

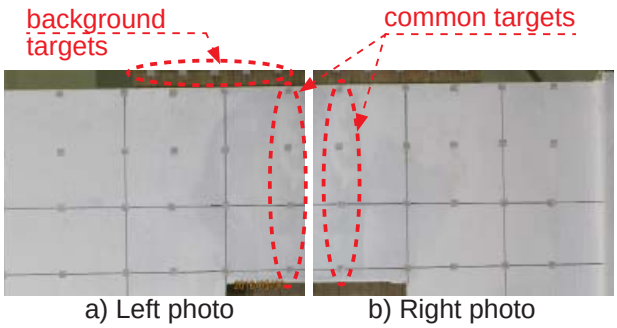

Fig. 5 Disposition of targets on before loading photos (Top floor beam - WD1)

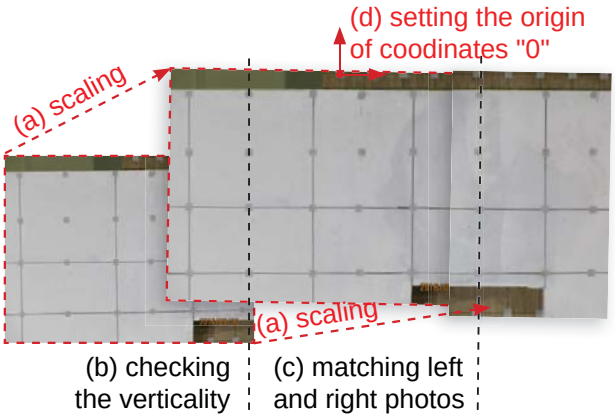

Fig. 6 Treatment process of the photos

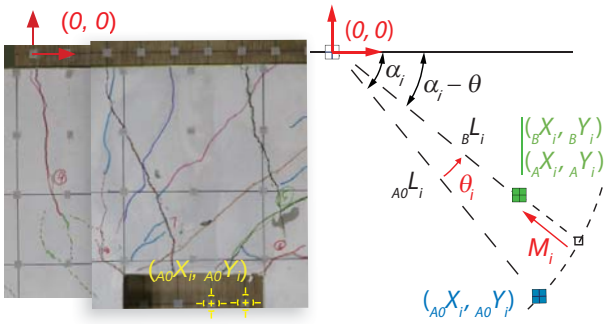

a) Location of background targets to be corrected

b) Correction of a target

Fig. 7 Background targets correction principle

the same treatment as the photos before loading. Nevertheless, when comparing the coordinates of the background targets common to the photos before and after loading (Fig.7a) and which are supposed to have the same coordinates, errors were observed. Those errors were caused by unexpected moves of the cameras between two photos taken and by some inaccuracy of the photos` treatments. By assuming that the coordinates of the photos before loading had the right coordinates, the photos after loading had to be corrected. Such correction was done as follow: (a) Calculate the distances from the origin of coordinates of the targets before loading ($_BL_i$ in Fig.7b) and those of the after loading ($_{A0}L_i$ in Fig.7b), using Eq. 1.

$$ {}_{A0}L_i = \sqrt{{}_{A0}X_i^{\,2} + {}_{A0}Y_i^{\,2}} \quad \text{and} \quad {}_{B}L_i = \sqrt{{}_{B}X_i^{\,2} + {}_{B}Y_i^{\,2}} \qquad (1) $$

(b) Calculate the ratios $M_i = {}_BL_i / {}_{A0}L_i$ for each target and their average M, which represents the difference of scale between the photos, using Eq. 2.

$$ M = \frac{1}{N}\sum_{i=1}^{N_w} \frac{{}_BL_i}{{}_{A0}L_i} \qquad (2) $$

N is the number of targets.

(c) Calculate the angle of rotation (θ_i in Fig.7b) of each target, and their average θ, using Eq. 3.

$$ \theta = \frac{1}{N}\sum_{i=1}^{N_w} \cos^{-1}\left[\frac{{}_BX_i \, {}_{A0}X_i + {}_BY_i \, {}_{A0}Y_i}{\sqrt{{}_BX_i^{\,2} + {}_BY^2}\cdot\sqrt{{}_{A0}X_i^{\,2} + {}_{A0}Y_i^{\,2}}} \right] \qquad (3) $$

(d) Find the correct coordinates of the targets after loading using Eqs 4 to 6:

$$ {}_AX_i = M\,{}_{A0}L_i \cos(\alpha_i - \theta) \qquad (4) $$

$$ {}_AY_i = M\,{}_{A0}L_i \sin(\alpha_i - \theta) \qquad (5) $$

with

$$ \alpha_i = \cos^{-1}\left[\frac{{}_{A0}X_i + {}_{A0}Y_i}{\sqrt{{}_{A0}X_i^{\,2} + {}_{A0}Y_i^{\,2}}} \right] \qquad (6) $$

$_{A0}X_i$,$_{A0}Y_i$: Targets` coordinates after loading, before correction.

$_AX_i$,$_AY_i$: Targets` coordinates after loading after correction. In the case of the background targets, $_AX_i$,$_AY_i$ are equals to the coordinates of the targets before loading $_BX_i$, $_BY_i$.

(e) Determine the horizontal and vertical displacements of each target, using Eq. 7:

$$ u_i = {}_AX_i - {}_BX_i \quad \text{and} \quad v_i = {}_AY_i - {}_BY_i \qquad (7) $$

To assess the accuracy of the results obtained with camera measurement method, the lateral displacements at mid height of the beam on the 3rd floor were gathered and are vertically illustrated in Fig.8. The values in blue represent the displacements at the left and right sides of the specimen, measured with LVDTs. The values in red are the displacements of targets measured with digital cameras. Though the position of the targets could not be measured with LVDTs, it is possible to assume an ideal, linear and constant displacement along the beam by interpolation. This ideal displacement is represented by the blue line in Fig.8. The accuracy of the noncontact measurement method is defined by the proximity of the measured values to the line. The average results, valued in percentage, give high accuracies of 94% in WD1 at positive cycle, 97% at

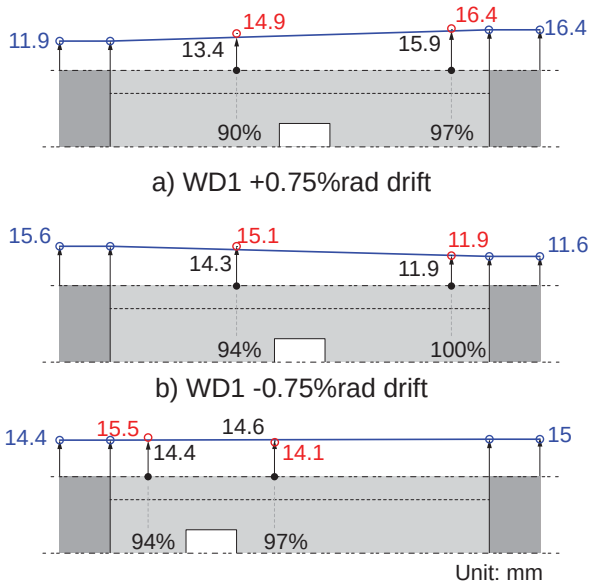

Fig. 8 Lateral displacements of the beam at the 3rd floor

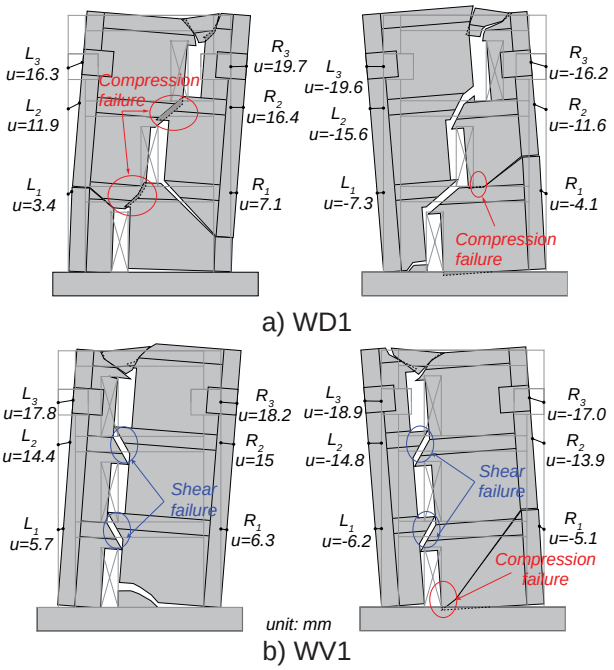

Fig. 9 Overall failure and lateral displacements at +0.75%rad (left) and -0.75%rad (right)

negative cycle and 96% in WV1 at positive cycle.

4. RESULTS

4.1 Concrete Failure Mode

Fig.9 shows the overall concrete failures in WD1 and WV1 specimens at +0.75% and -0.75% drift cycles. The values "*u*" represented at each floor are the horizontal displacements measured by LVDTs set on the lateral sides of the specimens.

The concrete of the intermediate beams in WD1 (see Fig.9a) is subjected to compression during positive loading cycle. This leads to spalling and complete crushing of the concrete on the beams during +0.1% loading cycle. During negative loading cycle, shear stresses are applied on the beams; In addition, compression failure also occurs at the bottom right corner of the 2nd floor opening. In WV1, shown in Fig.9b, the shear stresses occurring in the beams of the 2nd and 3rd floor, at both positive and negative cycles, cause the failure of specimen. Moreover, compression failure is observed on the wall, at the bottom right of the opening, at the 1st floor. Regarding the lateral displacements, they are closely symmetrical at positive and negative cycles, in both cycles. However, it is observed that the displacements in WV1 at the pushed sides are bigger that those of WD1 but smaller at the pulled sides. The phenomenon is explained by the different stresses within each specimen.

4.2 Cracks Distribution

Figs. 10 and 11 show the crack pattern in the beams of WD1 and WV1 up to -0.75% and +0.75%rad drifts. The blue arrows indicate the direction of the cracks on the walls as well as the distribution of the compression struts which vary depending on the position of the openings. The cracks in WD1 at positive cycle are widely spread both on the left and the right wall panels. The cracks at negative cycle however, are mostly located at the pushed wall panel. In that way, the crack distribution of the specimen at negative cycle is similar to that of WV1. The cracks distribution in the beams at the top floor and at the 3rd floor of the specimens are detailed in Figs. 12 to 15. Each Fig.was obtained following 3 steps: First, the beam was divided into several pieces according to the position of the major cracks. Secondly, for each part, one target located at the center of the part was defined as a rotation axes. Finally, the part was moved and rotated in order to match the position of the targets on the part with the exaggerated deformed shape of the beam. This exaggerated deformed shape was obtained using the displacements of the targets, magnified 10times.

Figs.12 and 13 detail the crack distribution in WD1 at respectively, +0.75% and -0.75% drift cycles.

At +0.75%, in the beam of the top floor (see Fig.12a), cracks show angles superior to 70° from the horizontal. Flexural damages are mostly located at the pulled side of the wall panel, at the corner of the opening. On the beam of the 3rd floor, for the same cycle (see Fig.12b), shear cracks are widely distributed on the beam, except on the area between the openings which is spared from any major cracks.

At -0.75% drift on the top floor beam (see Fig.13a), similarly to the opposite cycle, flexural cracks are located at the pulled side of the wall panel at the corner of the opening. However, during this cycle, the uplift of the beam, which is caused by the independent moves of the wall panels around the openings, is visually more evident than during the opposite cycle. The horizontal crack at the corner of the opening, at the pushed side of the wall panel, is the direct consequence of this uplift. In the beam of the 3rd floor (see Fig.13b), the distribution of the shear cracks is almost similar to the top floor beam. However, due to the existence of wall panels above the beam, the appearance of any flexural cracks was prevented. The cracks are mostly dispersed on the span between the two openings, about 350mm length, and in that way, contrasts with the cracks distribution during the positive loading cycle.

Figs. 14 and 15 show the cracks pattern in the beams of WV1 at respectively, +0.75% and -0.75% drift cycles. On the beam of the top floor, at both cycles (see Figs. 14a and 15), the cracks distribution is similar to that of WD1 on two points: First, the existence and location of the flexural cracks and the horizontal cracks; and secondly, the extent of the cracks to the nearest column. This concludes that the concrete damage of beams at roof floors follows the same pattern independently of the alignment of the openings. The cracks pattern in the beam of the 3rd floor at +0.75% drift cycle is shown in Fig.14b. The shear cracks, and in the same way, the concrete damages, are confined in the region between the openings.Consequently, the widths of the cracks

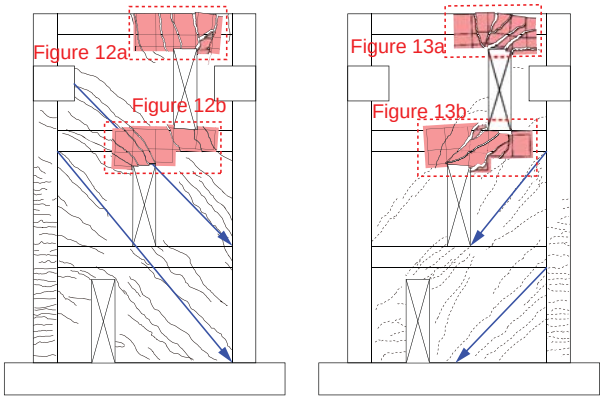

a) +0.75%rad b) -0.75%rad

Fig. 10 Crack pattern in WD1

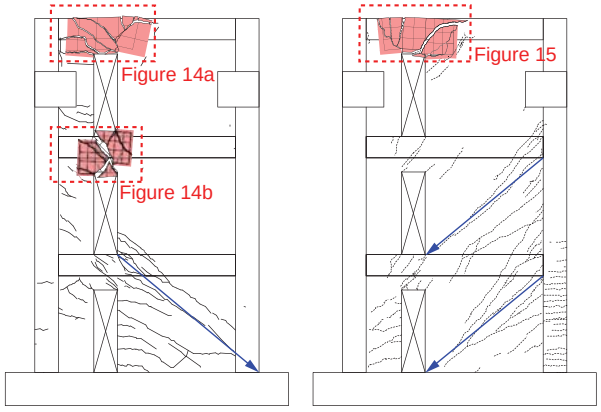

a) +0.75%rad b) -0.75%rad

Fig. 11 Crack pattern in WV1

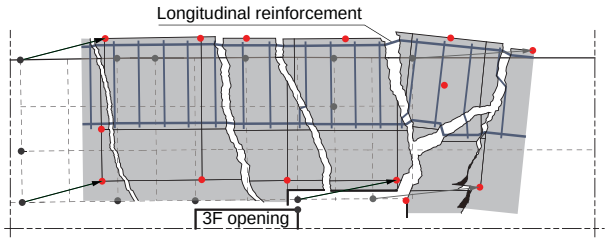

a) Top floor beam

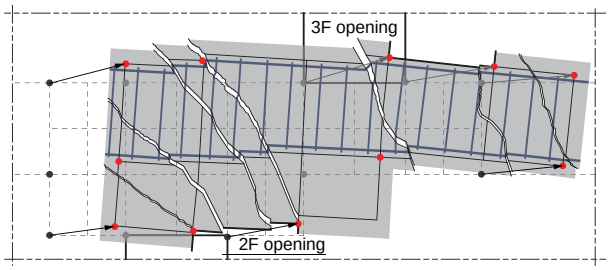

b) 3rd floor beam

Fig. 12 Beams concrete failure in WD1 (+0.75%rad)

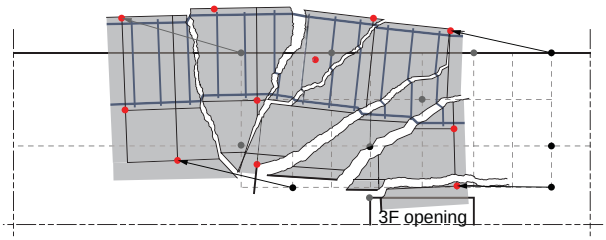

a) Top floor beam

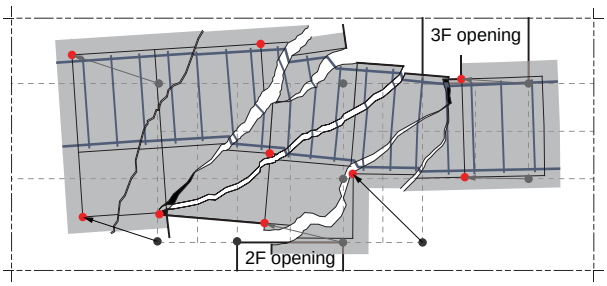

b) 3rd floor beam

Fig. 13 Beams concrete failure in WD1 (-0.75%rad)

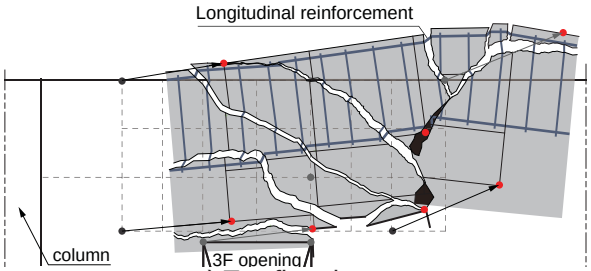

a) Top floor beam

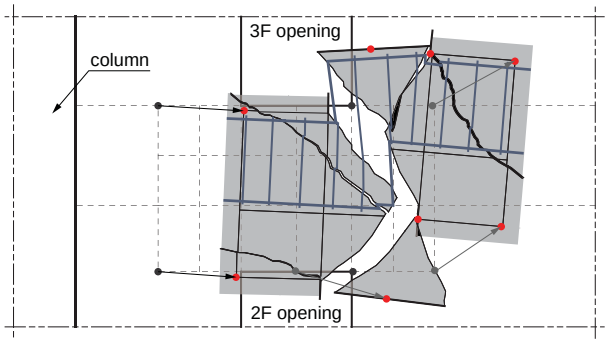

b) 3rd floor beam

Fig.14 Concrete failure mode - WV1 (+0.75%rad)

outside that area are almost negligible. Similar to the cracks distribution in WD1 specimen during negative cycle, the restriction of the cracks is caused by the existence of two wall panels above the beam, from either side of the opening. Unlike WD1 however, the distribution area of the concrete in WV1 is small (200mm), which explains the brittle behavior of the specimen (Fig.16). In addition, the downward and upward displacements of the left part and the right part of the cracked beam are more distinct than in WD1.

It was previously explained that the number of wall panels around the openings affects the cracks distribution in the beams. Therefore, it can be assumed that the cracks pattern in grade beams are

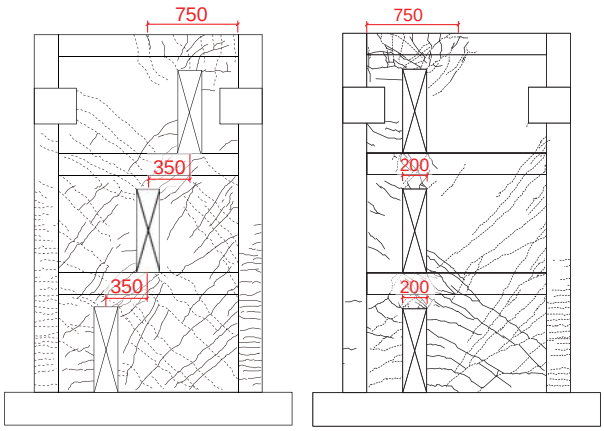

a) 365kN b) 241kN

Fig.16 Maximum shear capacities and disposition of the openings relationship

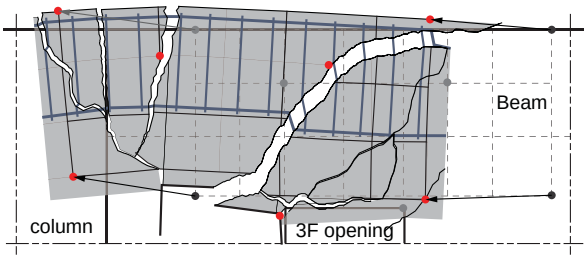

Fig. 15 Concrete failure mode - WV1 Top floor beam (-0.75%rad)

similar to the pattern in beams at roof floors, both being connected to two wall panels.

5. CONCLUSIONS

An experiment has been conducted on two multi-story RC shear walls with variable disposition of door openings. To discuss the two-dimensional deformations of the specimens, the displacements of the beams above the openings were measured with digital cameras. From this measurement, whose accuracy proved to be higher that 90% compared to results obtained with LVDTs, the following conclusions are obtained:

(1) For all loading directions, the cracks in the beams at the roof floor have different distribution compared to the cracks in the beams in intermediate floors.

(2) The occurrence of cracks in the beams of roof floors follows the same pattern, independently of the disposition of the openings on shear walls (Fig.16).

(3) The increase of the shear capacity in shear walls with door openings is caused by the increase of the size of the regions between the door openings (Fig.16).

REFERENCES

[1] AIJ Standard, Structural Calculation of Reinforced Concrete Structures, Architecture Institute of Japan, 2010.

[2] Hirosawa M., et al, "Structural Performance of Multi-Story RC Shear Walls with Multiple Door Openings (Part 1)", Proceedings of Tokai Chapter Architectural Research Meeting, Vol.55, pp.209-212, 2017. (in Japanese)

[3] S.Yoneyama, A.Kitagawa, "Bridge Deflection Measurement Using Digital Image Correlation with Camera Movement Correlation", Materials Transactions, Vol.53, No.2, pp.285-290, 2012.